A trajectory generation method for time-optimal helicopter shipboard landing

Di Zhao
PhD Student

Jayanth Krishnamurthi
PhD Candidate

Sandipan Mishra
Associate Professor

Farhan Gandhi
Redfern Chair in Aerospace Engineering

Rensselaer Polytechnic Institute
Troy, NY, United States

ABSTRACT

In this paper, a time-optimal trajectory generation algorithm is proposed for helicopter shipboard landing. The algorithm utilizes a simplified model of the helicopter's dynamics and exploits the differential flatness of the model to formulate a nonlinear programming problem, whose solution provides time-optimal reference approach/landing trajectories. The trajectories are then tracked by an inner-loop linear dynamic inversion (LDI) controller to generate the actual inputs that steer the full-state nonlinear helicopter model. The proposed algorithm reduces approach/landing flight time and enables a higher degree of maneuverability in comparison to typical state of the art methods of trajectory generation. Because of its computational efficiency, the path planner can also be used in real-time, i.e., through iterative recalculation of the remaining trajectory to account for deviations from the planned flight path. High fidelity simulations have been conducted on a verified UH-60A Black Hawk model, which show the effectiveness of the proposed method.

INTRODUCTION

Shipboard landing is among the most challenging helicopter flight operations (Ref. 1), because of the limited landing time, stringent safety constraints, rough sea conditions and turbulent shipboard motion, as well as complex ship-airwake-helicopter interactions during the landing maneuver.

As a result, there is significant pilot workload during the shipboard landing operation, which makes the development of the computer-assisted and/or fully autonomous control strategies imperative. Consequently, there has been substantial research effort towards designing effective control solutions for autonomous landing. In (Ref. 2), a novel control strategy was developed based on optical flow theory. A parameter *tau* inspired from human pilot behavior was defined to provide the guidance for relative motion between a target and the aircraft. Using this parameter was demonstrated to lead to a 'natural' and smooth autonomous landing. In (Ref. 3), a model predictive control (MPC) algorithm was proposed to deal with ship air wake and rough sea conditions during the landing process. Nonlinear simulations in that study proved the performance of the controller. In addition, efforts towards the application of the dynamic inversion (DI) controller on the ship-based helicopter were documented in (Refs. 4, 5). These controllers eliminated the need for the gain scheduling and controlled variables to follow commanded responses (Ref. 6). Human piloted and auto-piloted nonlinear simulations were conducted in (Ref. 4) and (Ref. 5) respectively, proving the effectiveness of the DI controller.

In contrast to the large body of research on the design of feedback controllers for helicopter shipboard landing, current trajectory generation methods for helicopter flight typically parameterize the reference trajectory with geometric or kinematic variables. Therefore, these trajectories normally do not guarantee time-optimality, lack lateral flexibility, and require manual tuning for specific parameters, often leading to conservative design of flight missions.

Recently, a methodology for formulating objective functions for optimized path guidance of helicopter shipboard landing was presented in (Ref. 7), where *optimal trajectory generation* ideas were developed. On the other hand, a new trajectory generation algorithm exploiting the differential flatness of the quadrotor dynamics was introduced in (Ref. 8), which proved to be computationally efficient in providing iterative real-time solution (in an MPC-like framework) when landing the quadrotor onto a moving platform, while respecting dynamics and actuator saturation constraints. The real time nature of this class of differential flatness based optimization algorithms makes it an attractive candidate for trajectory planning for helicopter maneuvers in general, and landing in particular; provided a differentially flat model of (simplified) nonlinear helicopter dynamics can be obtained.

Motivated by the need for trajectory planning methods for the helicopter shipboard landing problem, this paper presents a new time-optimal trajectory generation algorithm compatible with the standard cascade control structure (Ref. 5) for helicopters. The helicopter outer-loop dynamics are converted into an equivalent (and computationally efficient) model by exploiting the differential flatness property. This model is then used in the formulation of the trajectory optimization problem, which can be solved for a time-optimal reference trajectory. In addition, the corresponding (virtual) feedforward control command input for the inner-loop controller is

Presented at the AHS International 74th Annual Forum & Technology Display, Phoenix, Arizona, USA, May 14–17, 2018.

also generated by the proposed algorithm. A standard linear dynamic inversion (LDI) controller is used for inner-loop tracking control, which produces the actual input signals to the helicopter based on the command information from the outer-loop. Simulations conducted on the full-state nonlinear helicopter model validate the feasibility and effectiveness of the proposed algorithm.

HELICOPTER SHIPBOARD LANDING

Problem Statement

A schematic illustrating the helicopter shipboard landing problem is shown in Fig.1. Based on the measurement of both the fuselage state $\mathbf{x}_f$ and the shipboard state$\mathbf{x}_D$, the outer-loop path planner solves and stores the reference time-optimal trajectory, while the inner-loop controller generates the actual input that tracks the reference trajectory by using the information from the outer-loop. The helicopter is then steered to approach and land on the shipboard safely (by matching the shipboard and helicopter position, velocity, attitude, and rates there-of at the time of touchdown).

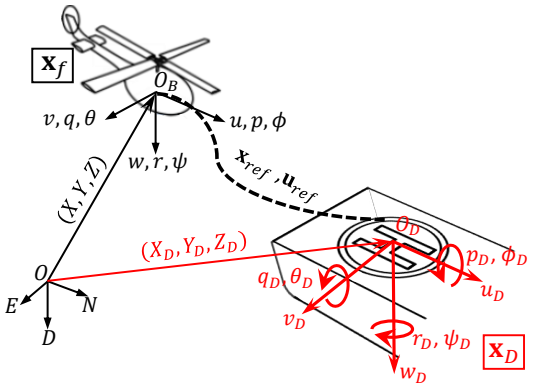

Fig. 1: Schematic of helicopter shipboard landing problem.

In order to succinctly describe the helicopter shipboard landing problem, the helicopter-shipboard system is separated into four subsystems including helicopter dynamics , shipboard kinematics, inner-loop linear dynamic inversion (LDI) controller and outer-loop path planner, in a cascaded control architecture shown in Fig.2.

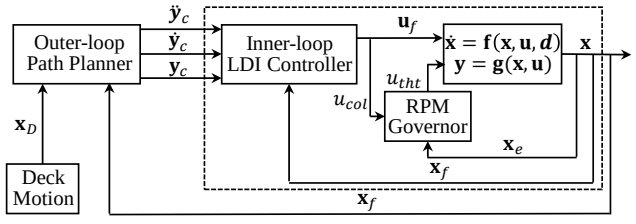

Fig. 2: Overall control architecture for helicopter shipboard landing.

The outer-loop path planner triggers the optimization algorithm when necessary to generate a reference trajectory based on current deck state $\mathbf{x}_D$ and fuselage state $\mathbf{x}_f$. Then, the above trajectory is stored so that the real time reference commands $\ddot{\mathbf{y}}_c$, $\dot{\mathbf{y}}_c$ and $\mathbf{y}_c$ can be time-scheduled and provided to the inner-loop controller, which uses an LDI control law to track these reference commands. Subsequently, the fuselage input $\mathbf{u}_f$ and the throttle input u_{tht} are generated by the inner-loop controller and RPM governor respectively, which steer the helicopter to the shipboard.

Next, we present a brief description of the helicopter dynamics, the shipboard motion, the ship-helicopter interaction. We then briefly present the inner-loop controller design. Finally, we propose a simplified outer-loop dynamic model and verify that it is indeed differentially flat.

Helicopter Dynamics

We use a UH-60A Black Hawk model developed by Krishnamurthi and Gandhi (Ref. 9), which is a derivative of Sikorsky's GenHel model (Ref. 10). The dynamics, in general, are given by

$$\begin{aligned} \dot{\mathbf{x}} &= \mathbf{f}(\mathbf{x}, \mathbf{u}, \mathbf{d}) \\ \mathbf{y} &= \mathbf{g}(\mathbf{x}, \mathbf{u}) \end{aligned} \tag{1}$$

where, $\mathbf{y}$ is the measurement of the states used in the controller, $\mathbf{x}$ is the state vector :

$$\mathbf{x} = \left[\mathbf{x}_f^T, \mathbf{x}_r^T, \mathbf{x}_t^T, \mathbf{x}_e^T\right]^T \tag{2}$$

$$\begin{aligned} \text{where} \quad \mathbf{x}_f &= \left[u, v, w, p, q, r, \phi, \theta, \psi, X, Y, Z\right]^T \\ \mathbf{x}_r &= \left[\beta_0, \beta_{1s}, \beta_{1c}, \beta_d, \dot{\beta}_0, \dot{\beta}_{1s}, \dot{\beta}_{1c}, \dot{\beta}_d, \lambda_0, \lambda_{1s}, \lambda_{1c}\right]^T \\ \mathbf{x}_t &= \lambda_{0_{TR}} \\ \mathbf{x}_e &= \left[\Omega, \chi_f, Q_e\right]^T \end{aligned} \tag{3}$$

$\mathbf{x}_f$ denotes 12 fuselage rigid body states, $\mathbf{x}_r$ denotes 8 blade flapping states and 3 inflow states of the main rotor, $\mathbf{x}_t$ denotes the tail rotor inflow state, $\mathbf{x}_e$ denotes 3 engine states.

The control input $\mathbf{u}$ is given by:

$$\mathbf{u} = \left[u_{lat}, u_{long}, u_{col}, u_{ped}, u_{tht}\right]^T \tag{4}$$

which consists of lateral, longitudinal, collective joystick input to the main rotor, pedal input to the tail rotor, and throttle input to the engine. Note that fuselage input $\mathbf{u}_f = \left[u_{lat}, u_{long}, u_{col}, u_{ped}\right]^T$ is comprised of the input channels governing the fuselage motion.

In this work, the disturbance $\mathbf{d}$ results from the ship-helicopter-airwake interaction, which will be introduced in a following subsection.

Shipboard Kinematics

The shipboard motion samples used in this study are based on the standard deck motion data for a generic surface combat ship. The data are extracted from the Systematic Characterization of the Naval Environment (SCONE) database developed by the Office of Naval Research (ONR) (Ref. 11).

In this work, shipboard motion characterized by dominant heave movement with low to medium intensity from the SCONE database are used as candidates. It was found that the time-varying deck height and heave rate can be well-approximated by explicit sinusoidal functions of the form:

$$F_{(\cdot)} = \bar{F}_{(\cdot)} + \sum_k A_{(\cdot),k} \sin(k\omega_{(\cdot)}t + \phi_{(\cdot),k}) \tag{5}$$

where $\bar{F}_{(\cdot)}$ is the time-average, ω is the frequency, $A_{(\cdot),k}$ and $\phi_{(\cdot),k}$ are the amplitude and phase lag related to the k^{th} harmonic, and $(\cdot)$ denotes either the deck height Z_D or the heave rate $\dot{Z}_D$. In this work, the above informations are retrieved from the SCONE data and known to the outer-loop path planner.

On the other hand, although the SCONE data also includes motion in other 5 degrees of freedom: surge, sway, roll, pitch and yaw, the intensities of the motions in these directions are low compared to the dominant heave motion. Hence, the horizontal motion of the ship is defined by a uniform forward speed at 20 knots (or 10.289 m/s) with a constant yaw angle, while the disturbances in sway, roll and pitch are ignored for the purposes of this study.

Helicopter-Shipboard Interactions

Ground Effect Model

The proximity of the helicopter to the deck of the ship alters the induced velocity in the plane of the rotor and affects rotor thrust and power, a phenomenon commonly known as ground effect. The ground effect model used is based on the source image approach given by Cheeseman and Bennett (Ref. 12) and implemented as a correction term which modifies the total resultant flow through the rotor disk (Ref. 13). The total non-dimensional resultant flow through the rotor disk out-of-ground effect (OGE) is calculated as

$$V_T = \sqrt{(-\mu_z + \lambda_m)^2 + \mu^2} \tag{6}$$

where λ_m denotes the non-dimensional induced velocity due to rotor thrust, μ and μ_z denote in-plane and climb velocities, respectively, in the wind axis of the rotor disk plane. With the helicopter in-ground effect (IGE), Eq.(6) is modified to include a correction term G as follows

$$\begin{aligned} V_T &= G\sqrt{(-\mu_z + \lambda_m)^2 + \mu^2} \\ G &= \frac{1}{1 - \frac{(-\mu_z+\lambda_m)^2}{16h^2(-\mu_z+\lambda_m)^2+\mu^2}} \end{aligned} \tag{7}$$

where h is the height of the rotor hub above the ground plane, normalized by rotor radius R.

Airwake Model

The implementation of the airwake simulation model is based on the work by Sparbanie (Ref. 14). The airwake flow field behind the ship's superstructure causes a change in the wind speed, which has deterministic and stochastic components. The deterministic component of the wind speed is given by

$$\bar{\mathbf{v}}_g^f = \left[\bar{u}_g^f, \bar{v}_g^f, \bar{w}_g^f\right]^T \tag{8}$$

where the superscript f denotes the quantities expressed in the helicopter body frame. These are determined by the mean wind speed of the airwake. On the other hand, the stochastic components of airwake are captured by the colored noise filters, which take the form

$$G_{(\cdot)}(s) = \frac{K_{(\cdot)}(s^2 + 2\zeta_{(\cdot),z}\omega_{(\cdot),nz}s + \omega_{(\cdot),nz}^2)}{(s^2 + 2\zeta_{(\cdot),p}\omega_{(\cdot),np}s + \omega_{(\cdot),np}^2)(s + p_{(\cdot)})} \tag{9}$$

where $(\cdot)$ denotes the elements in $\mathbf{v}_{gs}^f = \left[u_{gs}^f, v_{gs}^f, w_{gs}^f\right]^T$ and $\boldsymbol{\omega}_{gs}^f = \left[p_{gs}^f, q_{gs}^f, r_{gs}^f\right]^T$, which are the equivalent translational and rotational wind speed disturbances over the fuselage. In the simulation, the above components are obtained by exciting the filters with band-limited white noise. The local wind speed disturbances over a specific airframe component are given by $\mathbf{v}_{gs}^l = \left[u_{gs}^l, v_{gs}^l, w_{gs}^l\right]$, where the superscript l denotes the quantities expressed in the local frame of the component. These are calculated from the following equation

$$\mathbf{v}_{gs}^l = \mathbf{v}_{gs}^f + \boldsymbol{\omega}_{gs}^f \times \mathbf{r}_{l/f} \tag{10}$$

where $\mathbf{r}_{l/f} = \left[x_{l/f}, y_{l/f}, z_{l/f}\right]^T$ is the position vector from the local airframe component to the fuselage's center of gravity. Finally, the total airwake velocities in the local frame of the airframe component is simply the combination of the deterministic and stochastic components

$$\mathbf{v}_g^l = \mathbf{T}_{l/f}\bar{\mathbf{v}}_g^f + \mathbf{v}_{gs}^l \tag{11}$$

where $\mathbf{T}_{l/f}$ denotes the rotation tensor from fuselage to local coordinate frame.

It is important to note that the gust disturbances only affect the aerodynamic forces on the aircraft. The local airspeed velocity $\mathbf{v}_a^l = \left[u_a, v_a, w_a\right]^T$ on a specific airframe component is calculated by

$$\mathbf{v}_a^l = \mathbf{v}_i^l - \mathbf{v}_g^l \tag{12}$$

where $\mathbf{v}_i^l$ denotes the inertial velocity of the aircraft expressed in the local frame. The aerodynamic loads are calculated with the airspeed $\mathbf{v}_a^l$. The components of the dynamic model associated with the rigid-body equations of motion as well as the rotor inertial forces and flapping dynamics are independent of the surrounding airmass velocities and therefore only use $\mathbf{v}_i^l$.

In this work, a wind over deck (WOD) condition of 25 knots (or 12.8611 m/s)/0 deg on the Winston-Churchill Destroyer (DDG-81) is assumed to obtain the parameters in Eq.(9). The mean wind speed of the airwake is assumed to be uniform over the deck. To avoid sudden changes in the wind speed, the magnitude of the mean wind speed is linearly transitioned from 0 knots to 25 knots as the helicopter approaches from 200 ft (or 60.96 m) to 50 ft (or 15.24 m) away from the landing spot on the shipboard.

Inner-loop LDI controller

The design of the inner-loop controller is taken from (Ref. 9), based on the well-known model-following LDI control law.

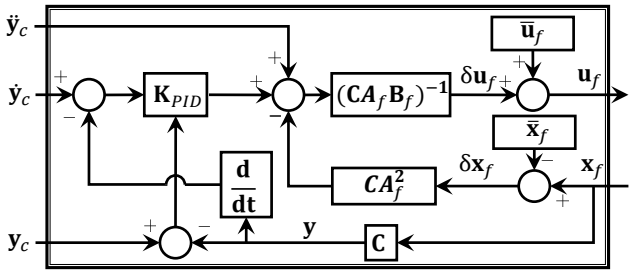

Fig. 3: Inner-loop LDI controller structure.

Fig.3 shows the structure of the controller, where the state space matrices $\mathbf{A}_f \in \mathbb{R}^{12\times12}$, $\mathbf{B}_f \in \mathbb{R}^{12\times4}$ are obtained by the linearization and order-reduction of the nonlinear model at different trim speeds. $\delta\mathbf{x}_f$ and $\delta\mathbf{u}_f$ are small perturbation from trim value $\bar{\mathbf{x}}_f$ and $\bar{\mathbf{u}}_f$ respectively. Moreover, the output command vector here is chosen as $\mathbf{y}_c = \left[\phi_c, \theta_c, -Z_c, \psi_c\right]^T$, which denotes the roll angle and pitch angle, the vertical velocity and the yaw angle respectively.

By implementing the $\mathbf{u}_f$ shown in Fig.3 onto the helicopter dynamics in Eq.(1), the dynamics of the error $\mathbf{e} = \mathbf{y}_c - \mathbf{y}$, (i.e. the difference between the output command and the actual output), become:

$$\ddot{\mathbf{e}} = \mathbf{K}_P\mathbf{e} + \mathbf{K}_I\int \mathbf{e}dt + \mathbf{K}_D\dot{\mathbf{e}} \tag{13}$$

The above dynamics are shaped by choosing proper PID gains, leading to the convergence of $\dot{\mathbf{y}}$ and $\mathbf{y}$ to $\dot{\mathbf{y}}_c$ and $\mathbf{y}_c$.

Simplified Dynamic Model for the Outer-Loop

With the inner-loop controller being responsive and robust, the subsystems in the dashed line box in Fig.(2) can actually be incorporated into one simplified dynamic model for the trajectory planner. These simplified dynamics are represented by

$$\dot{\mathbf{x}}_{ol} = \mathbf{f}_{ol}(\mathbf{x}_{ol}, \mathbf{u}_{ol}) \tag{14}$$

where $\mathbf{x}_{ol} = \left[\phi, \theta, \psi, X, Y, Z, \dot{\phi}, \dot{\theta}, \dot{\psi}, \dot{X}, \dot{Y}, \dot{Z}\right]^T$ is obtained by coordinate transformations of the translational and rotational rate in the fuselage state $\mathbf{x}_f$. On the other hand, the control input $\mathbf{u}_{ol} = \left[u_1, u_2, u_3, u_4\right]^T$ is chosen to be identical to the virtual input $\ddot{\mathbf{y}}$ of the inner-loop LDI controller. Hence:

$$\begin{aligned} \ddot{\phi} &= u_1 \\ \ddot{\theta} &= u_2 \\ \ddot{Z} &= -u_3 \\ \ddot{\psi} &= u_4 \end{aligned} \tag{15}$$

Note that Eq.(15) directly provides the simplified dynamic model of the helicopter attitude and vertical motion, leaving the dynamics of the horizontal motion to be determined next.

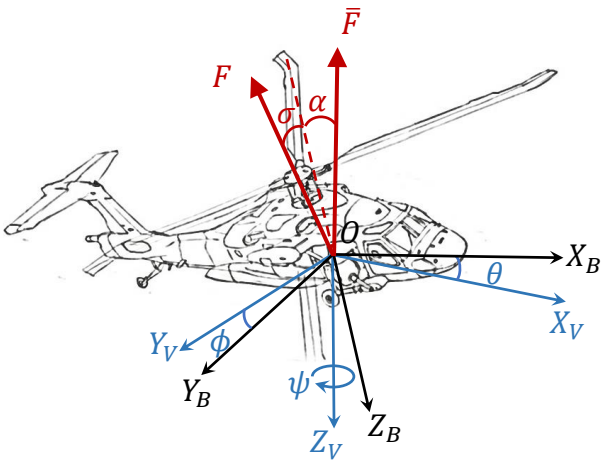

Fig. 4: Schematic of the helicopter coordinate systems

As shown in Fig.4, $OX_VY_VZ_V$ is the inertial frame with OX_V being the aircraft longitudinal axis' projection on the horizontal plane and OZ_V aligning with gravitational acceleration. $OX_BY_BZ_B$ is the aircraft body fixed frame. Notice that $OX_VY_VZ_V$ is transformed from North-East-Down(NED) inertial frame $OX_NY_EZ_D$ by $T_3(\psi)$ and $OX_BY_BZ_B$ is transformed from $OX_VY_VZ_V$ by $T_1(\phi)T_2(\theta)$.

In Fig.4, the non-gravitational resultant force $\bar{F}$ at trim attitude $(\bar{\phi}, \bar{\theta})$ points upward vertically and has the same magnitude of the gravitational force. With the control input perturbed from the trim condition, the helicopter reaches a new attitude (ϕ, θ), which leads to the rotation of the resultant force from $\bar{F}$ to F. The tilting of F can be described by the rotation $T_1(\sigma)T_2(\alpha)T_3(\psi)$ of the NED frame $OX_NY_EZ_D$. Therefore, the dynamics of the helicopter's translational motion in the NED frame are:

$$\begin{bmatrix} \ddot{X} \\ \ddot{Y} \\ \ddot{Z} \end{bmatrix} = \begin{bmatrix} 0 \\ 0 \\ g \end{bmatrix} + \frac{1}{m}\begin{bmatrix} T_{11} & T_{12} & \cos\sigma\sin\alpha\cos\psi + \sin\sigma\sin\psi \\ T_{21} & T_{22} & \cos\sigma\sin\alpha\sin\psi - \sin\sigma\cos\psi \\ T_{31} & T_{32} & \cos\sigma\cos\alpha \end{bmatrix}\begin{bmatrix} 0 \\ 0 \\ F \end{bmatrix} \tag{16}$$

We make the following assumptions to simplify this model:

1. The helicopter's vertical acceleration is small compared to gravitation acceleration, i.e. $\ddot{Z} \ll g$.
2. The trim values of roll and pitch angles $\bar{\phi}$ and $\bar{\theta}$ are small (within ±5 deg) throughout the flight.
3. The rotor thrust remains the dominant component of the resultant force F, of which the direction in the body fixed frame $OX_BY_BZ_B$ stays static.

Thus, with assumptions 2) and 3), we can claim that $\alpha \approx \theta - \bar{\theta}$ and $\sigma \approx \phi - \bar{\phi}$ and related terms in Eq.(16) can then be substituted. On the other hand, applying assumption 1) to the third equation expanded from Eq.(16), the resultant force F becomes:

$$F = -\frac{mg}{\cos(\phi - \bar{\phi})\cos(\theta - \bar{\theta})} \tag{17}$$

Replacing F in Eq.(16) with Eq.(17), the dynamic equations describing northward and eastward motion are written as:

$$\begin{aligned}\ddot{X} &= -g\left(\tan(\theta-\bar{\theta})\cos\psi+\frac{\tan(\phi-\bar{\phi})}{\cos(\theta-\bar{\theta})}\sin\psi\right)\\ \ddot{Y} &= -g\left(\tan(\theta-\bar{\theta})\sin\psi-\frac{\tan(\phi-\bar{\phi})}{\cos(\theta-\bar{\theta})}\cos\psi\right)\end{aligned} \tag{18}$$

which draws the implicit connection between helicopter horizontal motion and attitude. In summary, Eq.(15) and Eq.(18) together constitute the simplified dynamic model for the outer-loop path planner.

General formulation of the trajectory optimization problem

Before the discussion of differential flatness itself, we first state the motivation of invoking this property by introducing the general trajectory optimization problem.

Typically, the optimal control (or trajectory generation) problem can be stated as follows:

$$\begin{aligned}\min\quad & J = K\left(t_f,\mathbf{x}(t_f)\right)+\int_{t_0}^{t_f}L(t,\mathbf{x}(t),\mathbf{u}(t))\,dt\\ \text{subject to}\quad & \dot{\mathbf{x}}=\mathbf{f}(t,\mathbf{x}(t),\mathbf{u}(t))\\ & \mathbf{g}(t,\mathbf{x}(t),\mathbf{u}(t))\le\mathbf{0}\\ & \mathbf{k}(t_0,\mathbf{x}(t_0),t_f,\mathbf{x}(t_f))=\mathbf{0}\end{aligned} \tag{19}$$

where $\mathbf{x}(t)$ is the state trajectory, $\mathbf{u}(t)$ is the input trajectory, t_0 is the initial time, and t_f is the final time which can also be variable.

By solving the problem in Eq.(19), one can obtain the optimal input trajectory $\mathbf{u}^*(t)$ and the corresponding $\mathbf{x}^*(t)$ for $t\in[t_0,t_f^*]$. Such a solution minimizes the cost functional J, while satisfying the dynamics constraints, the algebraic path constraint and the boundary condition in Eq.(19).

However, it is computationally expensive to solve for $\mathbf{u}^*(t)$ directly, since Eq.(19) enforces a series of time-dependent equality constraints. Such a problem can be even more intractable when the dynamic constraint contains multivariate nonlinearities. Hence, it is preferable to convert Eq.(19) into some equivalent but computationally more tractable problem before attempting a numerical solution.

Differential flatness-based problem reformulation

Differential flatness of the outer-loop simplified dynamics

For the helicopter landing problem, a typical way to obtain the optimal trajectory is to formulate the dynamic constraint in Eq.(19) with the outer-loop simplified dynamics dictated by Eq.(14). However, as has been discussed above, the nonlinear equality constraints in Eq.(14) bring enormous cost to solving Eq.(19). Further, it will be later shown that not all the state variables in the above dynamics are required for determining the optimal trajectory.

Hence, instead of using Eq.(14) directly to form the dynamic constraints in the optimization problem, we will invoke the differential flatness property of the model to transform Eq.(14) into an equivalent system, which will prove to be computationally more efficient.

We now recall the definition of the differential flat system, as below (Ref. 15).

Definition: A system $\dot{\mathbf{x}}=\mathbf{f}(\mathbf{x},\mathbf{u})$ with $\mathbf{x}\in\mathbb{R}^n,\mathbf{u}\in\mathbb{R}^m$ is differential flat if there exists a flat output $\mathbf{y}\in\mathbb{R}^m$ in the form:

$$\begin{aligned}&\mathbf{y}=\Phi(\mathbf{x},\mathbf{u},\dot{\mathbf{u}},\cdots,\mathbf{u}^{(i)})\\ \text{such that}\quad &\mathbf{x}=\Phi_x(\mathbf{y},\dot{\mathbf{y}},\cdots,\mathbf{y}^{(j-1)})\\ &\mathbf{u}=\Phi_u(\mathbf{y},\dot{\mathbf{y}},\cdots,\mathbf{y}^{(j-1)},\mathbf{y}^{(j)})\end{aligned} \tag{20}$$

where Φ, Φ_x and Φ_u are smooth functions.

For the system represented by Eq.(14), the flat output can be chosen as:

$$\mathbf{y}_{ol}=\left[X,Y,Z,\psi\right]^T \tag{21}$$

Upon the selection of flat output $\mathbf{y}_{ol}$ in Eq.(21), the mappings from $\mathbf{y}_{ol}$, $\dot{\mathbf{y}}_{ol}$ and $\ddot{\mathbf{y}}_{ol}$ to $\left[\psi,X,Y,Z,\dot{\psi},\dot{X},\dot{Y},\dot{Z}\right]^T$ and $\left[u_3,u_4\right]^T$ are directly found, leaving the mappings to ϕ, θ and their time derivatives to be determined next.

Notice that Eq.(18) can be transformed into the form:

$$\begin{aligned}\theta &= -\arctan\left(\frac{\ddot{X}}{g}\cos\psi+\frac{\ddot{Y}}{g}\sin\psi\right)+\bar{\theta}\\ \phi &= \arctan\left(\frac{-\ddot{X}\sin\psi+\ddot{Y}\cos\psi}{\sqrt{g^2+(\ddot{X}\cos\psi+\ddot{Y}\sin\psi)^2}}\right)+\bar{\phi}\end{aligned} \tag{22}$$

Hence, the mappings to $\dot{\theta}$, $\dot{\phi}$, $\ddot{\theta}$ and $\ddot{\phi}$ can also be obtained by differentiating Eq.(22) once and twice respectively. Note that both X and Y are fourth-differentiable functions of time.

So far, the equivalent system of the one represented by Eq.(14) can be written explicitly in the linear Brunovsky form (Ref. 15):

$$\dot{\mathbf{q}}_{ol}=\mathbf{F}_{ol}\mathbf{q}_{ol}+\mathbf{G}_{ol}\mathbf{r}_{ol} \tag{23}$$

where the state vector $\mathbf{q}_{ol}=[X,\dot{X},\ddot{X},X^{(3)},Y,\dot{Y},\ddot{Y},Y^{(3)},Z,\dot{Z},\psi,\dot{\psi}]^T$ and the input vector $\mathbf{r}_{ol}=\left[r_1,r_2,r_3,r_4\right]^T=\left[X^{(4)},Y^{(4)},\ddot{Z},\ddot{\psi}\right]^T$, and:

$$\mathbf{F}_{ol}=\begin{bmatrix}\mathbf{J}_4 & \mathbf{0} & \mathbf{0} & \mathbf{0}\\ \mathbf{0} & \mathbf{J}_4 & \mathbf{0} & \mathbf{0}\\ \mathbf{0} & \mathbf{0} & \mathbf{J}_2 & \mathbf{0}\\ \mathbf{0} & \mathbf{0} & \mathbf{0} & \mathbf{J}_2\end{bmatrix},\quad \mathbf{G}_{ol}=\begin{bmatrix}\mathbf{L}_4 & \mathbf{0} & \mathbf{0} & \mathbf{0}\\ \mathbf{0} & \mathbf{L}_4 & \mathbf{0} & \mathbf{0}\\ \mathbf{0} & \mathbf{0} & \mathbf{L}_2 & \mathbf{0}\\ \mathbf{0} & \mathbf{0} & \mathbf{0} & \mathbf{L}_2\end{bmatrix} \tag{24}$$

$$\mathbf{J}_4=\begin{bmatrix}0&1&0&0\\0&0&1&0\\0&0&0&1\\0&0&0&0\end{bmatrix},\mathbf{L}_4=\begin{bmatrix}0\\0\\0\\1\end{bmatrix},\mathbf{J}_2=\begin{bmatrix}0&1\\0&0\end{bmatrix},\mathbf{L}_2=\begin{bmatrix}0\\1\end{bmatrix} \tag{25}$$

The input vector $\mathbf{u}_{ol}$ of the original system can be recovered from the input vector $\mathbf{r}_{ol}$ of the equivalent system by:

$$\begin{aligned}u_1 &= f_1(\mathbf{q}_{ol})+g_{11}(\mathbf{q}_{ol})r_1+g_{12}(\mathbf{q}_{ol})r_2\\ u_2 &= f_2(\mathbf{q}_{ol})+g_{21}(\mathbf{q}_{ol})r_1+g_{22}(\mathbf{q}_{ol})r_2\\ u_3 &= -r_3\\ u_4 &= r_4\end{aligned} \tag{26}$$

where f_1, f_2, g_{11}, g_{12}, g_{21} and g_{22} in Eq.(26) can be determined by the second differentiation of Eq.(22).

By representing the system in the form of Eq.(23), the original nonlinear dynamics in Eq.(14) are transformed into an equivalent set of linear kinematics, which is well-suited for trajectory planning and will be used to formulate the dynamic constraint in Eq.(19). On the other hand, the nonlinear terms in the original dynamics Eq.(18) are transferred into Eq.(22), which will be enforced by algebraic path constraint in Eq(19).

TIME-OPTIMAL TRAJECTORY GENERATION ALGORITHM FOR OUTER-LOOP PATH PLANNER

So far, a linear kinematic model that captures crucial characteristics of helicopter outer-loop motion has been developed. Next, based on the above model, corresponding cost function and multiple constraints are stated and formulated into an optimization problem, the solution of which generates the time-optimal reference trajectory for helicopter shipboard landing.

Cost function

The objective function of the optimization problem is the total approach time or landing flight time based on the specific scenarios, defined by:

$$\min \quad J = t_f - t_0, \tag{27}$$

where t_0 is the time at which the optimization algorithm is triggered, and t_f is the time instant (to be determined) when the helicopter reaches the terminal state (either end of landing or end of approach).

Discretized kinematics

For computational tractability, the infinite dimensional optimization problem in Eq.(19) is converted to a finite dimensional one by discretization. Here, the trajectory being optimized is discretized into N segments, which is preselected. Hence, the sampling time t_s is:

$$t_s = \frac{t_f - t_0}{N-1} \tag{28}$$

Then, by assuming the input $\mathbf{r}_{ol}$ to be zero-order hold (ZOH) signal, the continuous kinematics in Eq.(23) can be discretized by:

$$\mathbf{q}(k+1) = \mathbf{F}\mathbf{q}(k) + \mathbf{G}\mathbf{r}(k) \tag{29}$$

where $\mathbf{q}(k) = [X(k), X_v(k), X_a(k), X_j(k), Y(k), Y_v(k), Y_a(k), Y_j(k), Z(k), Z_v(k), \psi(k), \psi_v(k)]^T$ is the discretized state vector and $\mathbf{r}(k) = [X_s(k), Y_s(k), Z_a(k), \psi_a(k)]^T$ is the discretized input vector at the k^{th} node. The subscripts v, a, j and s represent velocity, acceleration, jerk and snap respectively.

Altogether, the optimization variables are comprised of t_f, $\mathbf{q}(k)$ and $\mathbf{r}(k)$ for all $k \in [1, N] \subseteq \mathbb{N}$, of which the concatenated vector belongs to $\mathbb{R}^{(16N+1)\times 1}$.

Optimization constraints

The optimization constraints used for the optimizer are listed below in entirety, of which some may be activated for the approach and others for the landing trajectory generation.

Discretized kinematics constraints: The kinematics in Eq.(29) governing the forward propagation of the trajectory should be always satisfied during the optimization process, that is:

$$\mathbf{q}(k+1) - \mathbf{F}\mathbf{q}(k) - \mathbf{G}\mathbf{v}(k) = \mathbf{0}, \ \forall k \in [1, N-1] \subset \mathbb{N} \tag{30}$$

Boundary condition constraints: The initial and terminal condition constraints have the generalized form:

$$\mathbf{q}(1) = \mathbf{q}_0, \ \mathbf{q}(N) = \mathbf{q}_f \tag{31}$$

The initial condition $\mathbf{q}_0$ is decided by the fuselage state $\mathbf{x}_f$ at t_0 when the algorithm is executed. All terminal conditions in $\mathbf{q}_f$ except for vertical motion terms are dictated by the deck motion state $\mathbf{x}_D$ and its time derivatives at the terminal time t_f. Note that high-order time derivatives including X_{j0}, Y_{j0}, X_{jf} and Y_{jf} in $\mathbf{q}_0$ and $\mathbf{q}_f$ are set free.

On the other hand, Z_f and Z_{vf} are chosen differently for the approach and landing scenarios. For the approach trajectory, the helicopter ends up hovering at some predetermined altitude, which makes:

$$Z_f = \bar{F}_{Z_D} + Z_{HOV}, \ Z_{vf} = 0 \tag{32}$$

where Z_{HOV} is set to $-6m$ for all approach trajectories in this paper. For the landing trajectory, the helicopter is required to touch down on the deck with zero vertical relative velocity, which makes:

$$Z_f = Z_{TOL} + F_{Z_D}(t_f), \ Z_{vf} = F_{\dot{Z}_D}(t_f) \tag{33}$$

where Z_{TOL} is the landing safety tolerance accounting for helicopter size (i.e. distance from the center of gravity to the landing gear plane) and other safety redundancies, $F_{Z_D}(t_f)$ and $F_{V_{ZD}}(t_f)$ are given by Eq.(5).

By splitting the entire flight trajectory into approach/landing phases and setting different terminal constraints for vertical motion, the optimizer is freed from solving for the terminal deck height $F_{Z_D}(t_f)$ and heave rate $F_{V_{ZD}}(t_f)$ during the approach trajectory planning, which saves computational cost.

Input constraints: Ideally, the input constraints should be implemented by setting upper and lower bounds directly for Eq.(26); however, the computational cost of iteratively solving for u_1 and u_2 in Eq.(26) is enormous because of the complexity of these functions. On the other hand, it is easy to show that u_1 and u_2 can be bounded by simply constraining $\dot{X}$, $X^{(3)}$, $X^{(4)}$, $\dot{Y}$, $Y^{(3)}$, $Y^{(4)}$, $\dot{\psi}$ and $\ddot{\psi}$. Hence, the constraints of u_1 and u_2 are transferred to the constraints of other states and inputs, leaving the input constraint to be:

$$|\mathbf{r}^{sub}(k)| \leq \mathbf{r}^{sub}_{\max}, \forall k \in [1, N] \subset \mathbb{N}. \tag{34}$$

where $\mathbf{r}^{sub}(k) = \left[Z_a(k), \psi_a(k)\right]^T$.

State constraints: The state constraints are written as:

$$|\mathbf{q}^{sub}(k)| \leq \mathbf{q}^{sub}_{\max}, \forall k \in [1,N] \subset \mathbb{N}. \tag{35}$$

where $\mathbf{q}^{sub}(k) = \left[Z_v(k), \psi_v(k), X_j(k), Y_j(k), X_s(k), X_s(k)\right]^T$. Except for the above states, the horizontal velocity $V(k)$, the roll angle $\phi(k)$ and pitch angle $\theta(k)$ are also constrained by:

$$\mathbf{h}_{\min} \leq \mathbf{h}(\mathbf{q}(k)) \leq \mathbf{h}_{\max}, \forall k \in [1,N] \subset \mathbb{N}. \tag{36}$$

where $\mathbf{h}(\mathbf{q}(k))$ includes $V(k) = \sqrt{X_v^2(k) + Y_v^2(k)}$ and Eq.(22).

Additional constraints: Aside from the above common constraints, scenario specific constraints must also be enforced for the different flight phases.

The horizontal airspeed is comparatively high during approach, so that the side-slip angle is constrained by:

$$\begin{gathered}\beta(k) = \psi(k) - \arctan 2(Y_v(k), (X_v(k)) = 0, \\ \forall k \in [1,N] \subset \mathbb{N}.\end{gathered} \tag{37}$$

Moreover, there may exist aggressive horizontal maneuvers that make the snaps X_s and Y_s have discontinuities or chatter during approach, hence a finite impulse response (FIR) filter is used to filter out high frequency components in these signals:

$$\begin{gathered}|\frac{X_s(k+1) + X_s(k-1)}{2} - X_s(k)| \leq \tilde{X}_{s\max}, \\ |\frac{Y_s(k+1) + Y_s(k-1)}{2} - Y_s(k)| \leq \tilde{Y}_{s\max}, \\ \forall k \in [2,N-1] \subset \mathbb{N}.\end{gathered} \tag{38}$$

On the other hand, to improve the landing safety, additional constraints are enforced on landing trajectory. Anti-collision constraint is implemented by:

$$Z(k) \leq Z_{TOL} + F_{Z_D}(kt_s), \forall k \in [1,N] \subset \mathbb{N}. \tag{39}$$

where $F_{Z_D}(kt_s)$ is the deck height sampled at the k^{th} time step.

Due to model inaccuracy, actuator delay and possible deck rolling/pitching, there will inevitably be some relative velocity between the helicopter and the deck at touch down. Such situations can be remedied by picking a window time when the deck motion is relatively quiescent for the helicopter to land. This is achieved by constraining the absolute value of deck heaving rate at the touch down time instant:

$$|F_{\dot{Z}_D}(t_f)| \leq \dot{Z}_{D\max} \tag{40}$$

where $\dot{Z}_{D\max}$ is the threshold constant that can be tuned for different conditions.

Formulation of the optimization problem

With the cost function and optimization constraints listed above, the optimization problem can be written as:

$$\begin{aligned} \underset{t_f, \mathbf{q}(k), \mathbf{r}(k)}{\arg\min} \quad & J = t_f - t_0 \\ s.t \quad & \Gamma_{\min} \leq \Gamma(t_f, \mathbf{q}(k), \mathbf{r}(k)) \leq \Gamma_{\max}, \\ & \Gamma^{ap}_{\min} \leq \Gamma^{ap}(t_f, \mathbf{q}(k), \mathbf{r}(k)) \leq \Gamma^{ap}_{\max}, \\ & \text{if approach.} \\ & \Gamma^{ld}_{\min} \leq \Gamma^{ld}(t_f, \mathbf{q}(k), \mathbf{r}(k)) \leq \Gamma^{ld}_{\max}, \\ & \text{if landing.} \end{aligned} \tag{41}$$

where Γ is the constraint function with Eq.(30), Eq.(31) and Eq.(34)-Eq.(36) stacked up together, Γ^{ap} is comprised of Eq.(37)-Eq.(38), Γ^{ld} is comprised of Eq.(39) and Eq.(40). Note that "$\leq$" denotes element-wise inequality and 0s are used for both the lower and upper bounds of the equality constraints in Eq.(41).

In this work, the optimization problem Eq.(41) is solved using numerical optimization tool CasADi in MATLAB, with the 'IPOPT' solver.

Generation of the control commands

The control commands generation process is shown in Fig.5.

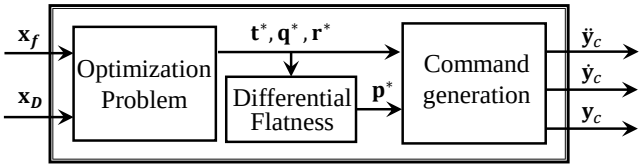

Fig. 5: Outer-loop path planner structure.

Upon the solving of the optimization problem in Eq.(41), the optimization variables $\left[t_f^*, \mathbf{q}^*(k), \mathbf{r}^*(k)\right], \forall k \in [1,N] \subset \mathbb{N}$ are obtained, with the corresponding reference time sequence defined by:

$$\mathbf{t}^*(k) = t_0 + (k-1)t_s, \forall k \in [1,N] \subset \mathbb{N}. \tag{42}$$

where t_s is calculated by Eq.(28). Then, benefited from the differential flatness of the system, the optimal roll and pitch motion $\mathbf{p}^*(k) = \left[\phi^*(k), \theta^*(k), \dot{\phi}^*(k), \dot{\theta}^*(k), \ddot{\phi}^*(k), \ddot{\theta}^*(k)\right]$ can be obtained, by first calculating roll and pitch angles via Eq.(22) and then differencing them to get higher order time derivatives. Then, $\left[\mathbf{t}^*(k), \mathbf{p}^*(k), \mathbf{q}^*(k), \mathbf{r}^*(k)\right]$ is stored as a reference trajectory. At each time step, the control commands $\ddot{\mathbf{y}}_c$, $\dot{\mathbf{y}}_c$ and $\mathbf{y}_c$ are scheduled from the reference with the current flight time. Further, errors in horizontal position and velocity are compensated by an outer-loop LDI controller similar to the one used in (Ref. 9).

SIMULATION RESULTS

In this section, we present results from simulation of a variety of landing scenarios and the performance of the proposed algorithm under these scenarios.

Flight scenarios

Approach phase

Three cases of flight approach scenarios with different initial shipboard states listed in Table 1 have been used for testing the approach trajectory generation capability of the proposed algorithm. Note that the helicopter starts all three flights at (0m,0m,-70m) in the NED frame with a trim condition at 80 knots (41.156 m/s).

Table 1: Initial shipboard states in different flight scenarios for approach.

case #	North position (m)	East position (m)	Heading angle (deg)
1	500	0	0
2	500	350	0
3	350	350	30

Landing phase

Two cases of landing scenarios with different shipboard heave motion intensities have been used for testing the landing trajectory generation capability of the proposed algorithm. In this work, all landing trajectories start at the terminal state of the approach trajectory in case 3 of Table 1.

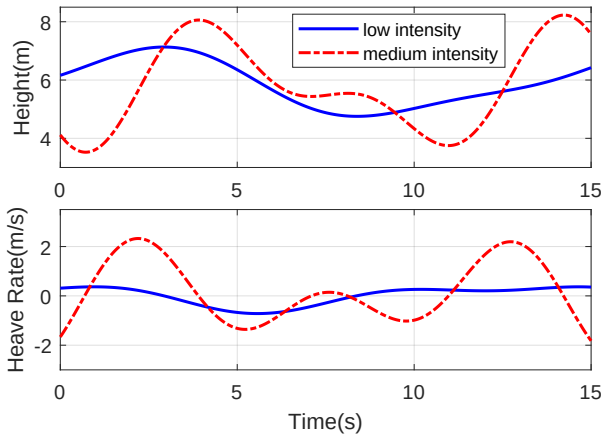

Fig. 6: Shipboard heave motion samples.

The two samples of shipboard used in the simulations are shown in Fig.6. These samples are generated using Eq.(5).

Reference trajectories generated by the proposed algorithm

Approach phase

Fig.7 shows the ground tracks of the reference approach trajectories generated by the proposed algorithm in all three cases.

In all three cases, the helicopter has a successful rendezvous with the ship with the heading angle aligned. The

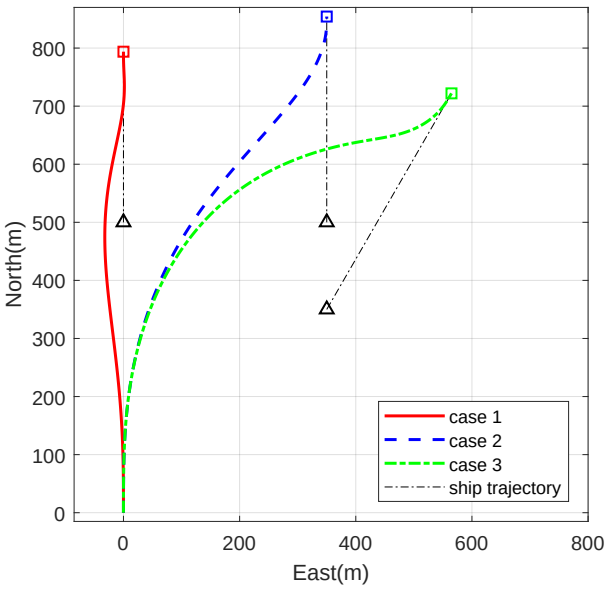

Fig. 7: Ground tracks of the approach trajectories.

ability of the proposed algorithm to plan for different flight scenarios with high degree of flexibility is thus demonstrated.

Fig.8 shows the altitude and airspeed profiles of the reference trajectories. In all three cases, the helicopter descends to the prescribed hover altitude, while decelerating to the same speed as the ship at the end of the approach phase. Note that the proposed algorithm has different deceleration strategies for different flight scenarios so that the flight time can be minimized, while satisfying all the constraints.

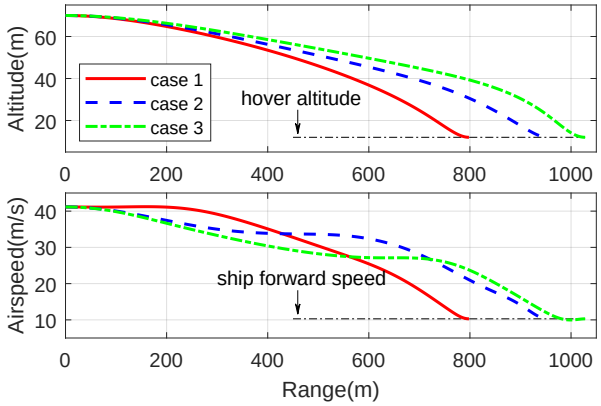

Fig. 8: Altitude and airspeed versus range profiles during approach.

Fig.9 shows the corresponding helicopter attitudes time-trace during the approach. In all three cases, the roll and pitch angles are well constrained by Eq.(36). Moreover, the anti-sideslipping constraint Eq.(37) enforces the yaw angle to align with the flight azimuth angle throughout the approach.

Fig.10 shows the comparison between the computational time for the proposed algorithm against the "standard" algorithm (i.e. formulating the dynamic constraint in Eq.(19) by directly using Eq.(14) instead of Eq.(23)). The result is obtained by solving the trajectory for case 3 using randomized

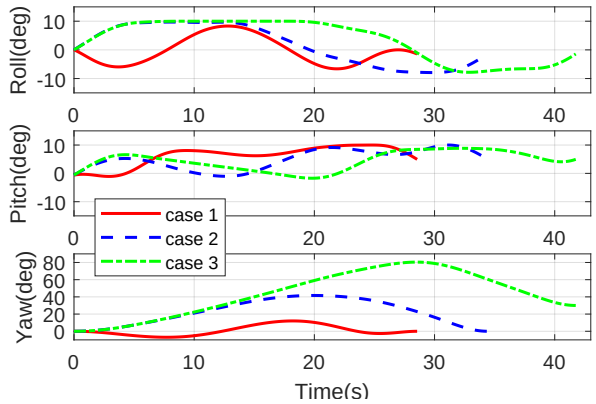

Fig. 9: Helicopter attitude time histories during approach.

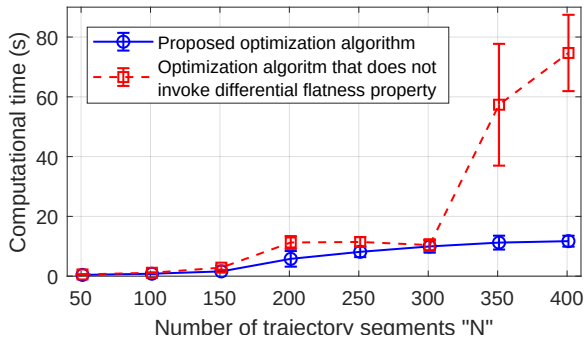

Fig. 10: Computational time comparison between the proposed algorithm and the one that does not invoke differential flatness property.

initial guesses, on a laptop with Intel Core i5-6200U 2.40 GHz.

Overall, the proposed algorithm has higher computational efficiency compared to the "standard" algorithm . As the number of trajectory segments N increases from 50 to 300, the computational time taken by the proposed algorithm increases gradually from 0.5 second to 10 seconds. On the other hand, the "standard" algorithm takes much larger computational effort to converge for N larger than 300. Furthermore, the "standard" algorithm's computational time is very sensitive to different initial guesses.

Landing phase

Fig.11 and Fig.12 show the reference trajectories for landing on the shipboard with low and medium heave motion intensities respectively.

Although all trajectories satisfied terminal position and velocity constraints, the trajectories without constraints on the terminal deck heaving rate appear to be much more aggressive, which corresponds with minimum landing time. On the other hand, the two gentler trajectories hover longer and seek to land when the deck heaving is more quiescent.

For all the landing cases shown above, we use $N = 101$ trajectory segments, leading to an average computational time of 0.5 seconds, which illustrates that the proposed algorithm can be used in real-time iteratively.

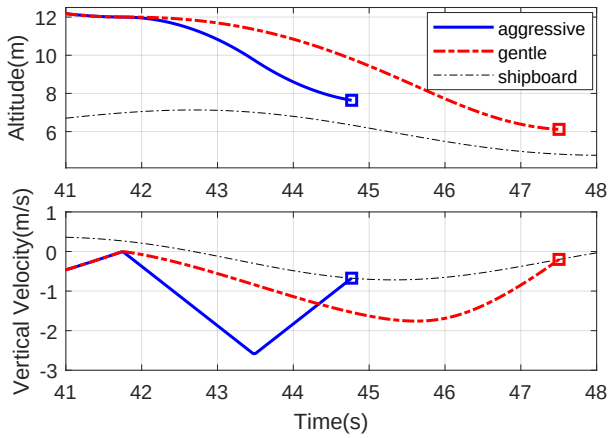

Fig. 11: Reference trajectories for landing on the shipboard with low heave motion intensity.

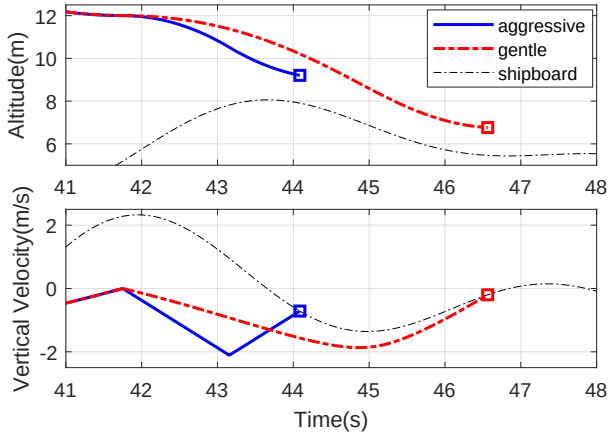

Fig. 12: Reference trajectories for landing on the shipboard with medium heave motion intensity.

Implementation on the nonlinear full-state model simulation

Approach phase

All three reference approach trajectories generated in the previous section have been implemented on the nonlinear helicopter simulation model (with the inner-outer loop structure described in Fig.3). Flights with and without the presence of the ship airwake have both been tested. However, for clarity, Fig.13, Fig.14 and Fig.15 only show the simulation results from case 3 in Table 1. On the other hand, Table 2 lists the terminal errors of actual approach trajectories for all three cases.

Fig.13 shows the simulation results of the helicopter position during the approach. In both flight simulations with and without airwake effects, the actual positions track the reference tightly. This is a result of both effectiveness of the outer-loop path planner as well as the responsiveness of the inner-loop LDI controller.

Fig.14 shows the simulation results of the helicopter attitude during the approach. In the simulation without the airwake, all three Euler angles follow the reference closely. This indicates the high prediction accuracy of Eq.(22), which has

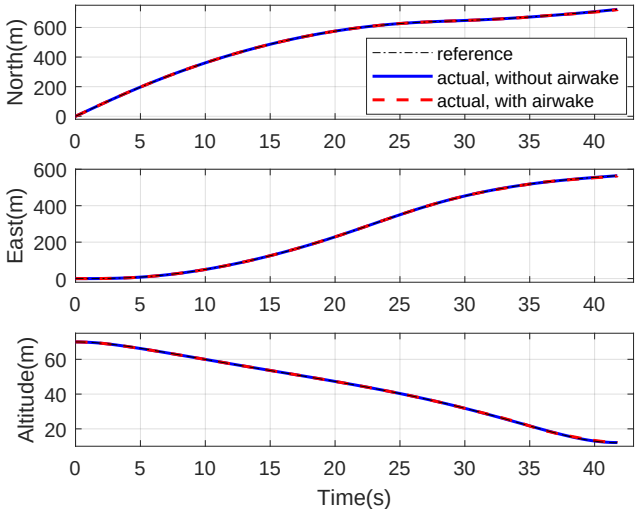

Fig. 13: Tracking history of the helicopter position during the approach.

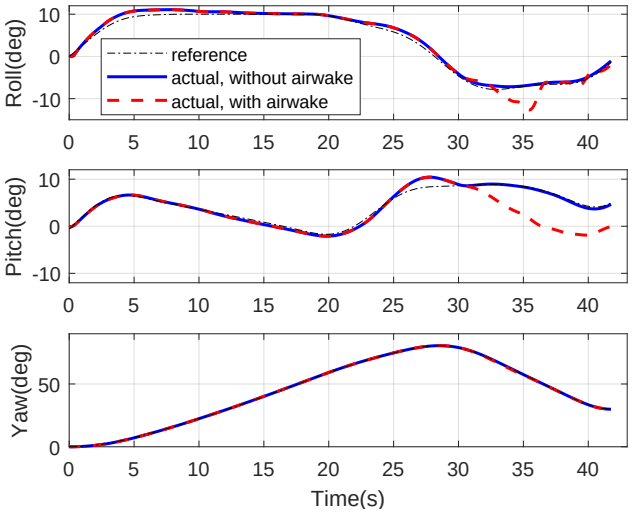

Fig. 14: Tracking history of the helicopter attitude during the approach.

generated reference roll and phi angles by only using the information extracted from the flat output.

On the other hand, in the simulation with airwake effects, the roll and pitch angles do not follow the reference well after the helicopter enters the ship airwake region. Under such circumstances, the trim roll and pitch angles used in Eq.(22) are no more accurate due to the 25 knots head wind. Hence, the actual roll and pitch angles flown are mainly dictated by the outer-loop LDI controller in order to compensate for the horizontal position and velocity errors.

Fig.15 shows simulation results of the actuator states during the approach. Here, the influence of the ship airwake is further highlighted. Compared to the smooth actuator states in the two cases without the presence of the ship airwake, the ones under the influence of the airwake become rougher when the helicopter is near the shipboard. This occurs because the inner-loop controller is trying to reject the stochastic aerodynamic loads caused by the airwake.

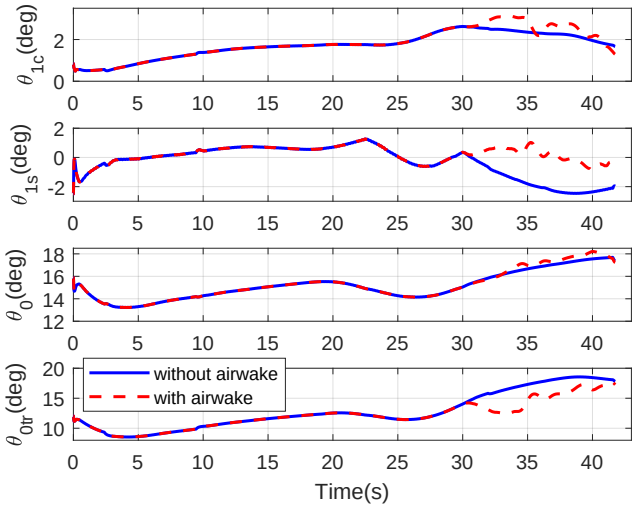

Fig. 15: Actuator states of main rotor and tail rotor during the approach.

Table 2: Terminal errors of the approach trajectories.

case #	horizontal position (m)	vertical position (m)	horizontal velocity (m/s)	vertical velocity (m/s)	heading angle (deg)
1	1.1197	0.0463	0.2053	0.0154	0.0864
1*	2.2024	0.1490	0.8576	0.1063	0.2258
2	0.8393	0.0857	0.2010	0.0133	0.0102
2*	2.1688	0.0283	0.4983	0.1250	0.0800
3	0.4180	0.1248	0.1242	0.0253	0.1041
3*	0.9370	0.1518	0.5388	0.1066	0.1976

Cases with $*$ are results from the simulations with the presence of the ship airwake.

As can be seen in Table 2, those trajectories simulated without airwake's influence have smaller terminal errors in both horizontal position and velocity. However, in general, the helicopter ends up considerably close to the desired states prescribed by the reference trajectories in all the cases simulated. Hence, despite the difference of the flight scenarios, the actual fuselage state of helicopter relative to the ship is basically the same at the end of the approach, which simplifies the landing trajectory planning significantly.

Landing phase

All four reference landing trajectories shown in Fig.11 and Fig.12 have been implemented on the nonlinear helicopter model. Similar to the approach phase, flights with and without the ship airwake have both been tested. For clarity, Fig.16 and Fig.17 only show the simulation results of the two trajectories shown in Fig.12, while Table 3 lists helicopter's state relative to the shipboard at touchdown for all the cases simulated.

Fig.16 shows the helicopter's vertical motion during landing. Due to the factors such as actuator delay, the helicopter cannot accelerate and decelerate as swiftly as planned by the proposed algorithm. Therefore, in both flights with and without airwake, it is more difficult for helicopter to follow the more aggressive trajectory, which leads to the touch downs ahead of schedule and the comparatively larger relative nor-

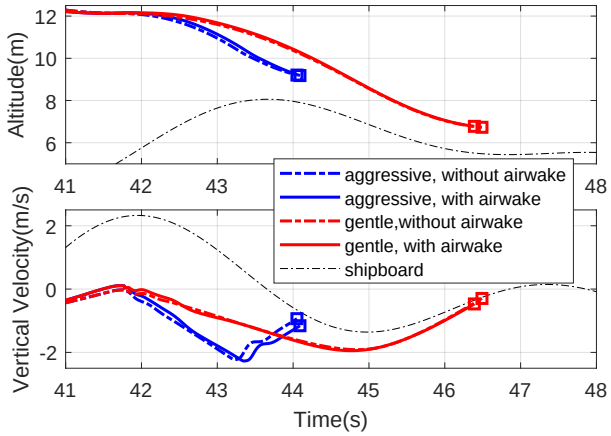

Fig. 16: History of the vertical motion during landing on the shipboard with medium intensities.

mal velocity to the deck compared to the one of the gentle trajectory.

On the other hand, the presence of the airwake also influences helicopter's vertical motion. Due to the wind speed changes, the control of the vertical motion is seen to be less effective. Hence, compared to the landings without any airwake effects, the helicopter's states deviate more from the reference trajectory. Further, this influence is more evident in the aggressive landing scenario, as the controller has less control margin to reject the perturbations when it is executing aggressive maneuvers.

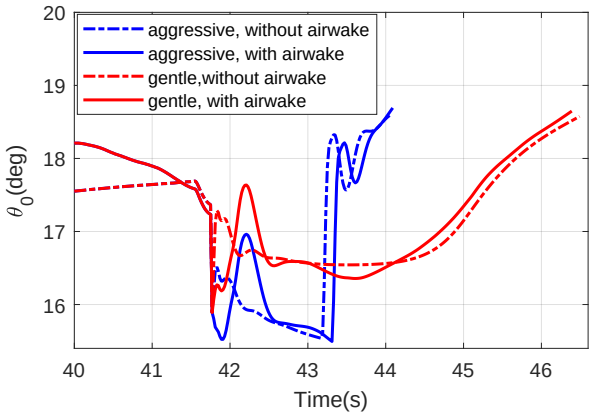

Fig. 17: Collective pitch angle of the main rotor during landing on the shipboard with medium intensities.

Fig.17 shows the corresponding collective pitch angle of the main rotor of the four landing cases shown in Fig.16. The large change of the collective pitch angle during the aggressive landing is essentially a result from the bang-bang control input of the vertical acceleration (which achieves the time optimality). This bang-bang behavior is notably absent during the gentle landings, which trade-off landing time for a softer touchdown. On the other hand, for landing with airwake, the collective pitch angle is actuated more drastically in order to adjust to the stochastic wind speed perturbation.

As can be seen in Table 3, aggressive landings typically end with higher normal speed to the deck at touchdowns compared to the gentle ones. Such decrease in the normal speed is more obvious when the helicopter is landing on the shipboard with medium heave intensity.

Table 3: State of the helicopter relative to the shipboard at touchdown.

case #	landing strategy	landing position (m)	tangential velocity (m/s)	normal velocity (m/s)	heading angle (deg)
1	gentle	0.0805	0.0699	0.2136	0.0598
1*	gentle	0.2647	0.1819	0.1528	0.1137
1	aggressive	0.2414	0.1429	0.4835	0.0279
1*	aggressive	0.1937	0.1660	0.4806	0.0188
2	gentle	0.1076	0.0958	0.0346	0.0401
2*	gentle	0.1676	0.2160	0.1181	0.0204
2	aggressive	0.2494	0.1279	0.2724	0.0284
2*	aggressive	0.2300	0.2309	0.4382	0.0562

Case 1 and case 2 denote landing on the shipboard with low and medium heave intensities respectively. Cases with $*$ are results from the simulations with the presence of the ship airwake.

CONCLUSIONS

In this paper, a time-optimal trajectory generation algorithm for helicopter shipboard landing is proposed. By utilizing the equivalent model converted from the simplified helicopter dynamics via differential flatness, together with the introduction of corresponding cost function and constraints, the algorithm formulates a standard optimization problem, which can be solved efficiently for the time-optimal reference trajectories capable of obstacle avoidance and large heading maneuvers. The proposed algorithm is compatible with the standard LDI controller, which is used to track the references. Simulations conducted on a full-state nonlinear helicopter model, together with the presence of helicopter-shipboard interactions, show the effectiveness of the proposed method.

Author contact information: Di Zhao, zhaod3@rpi.edu; Jayanth Krishnamurthi, krishj@rpi.edu; Sandipan Mishra, mishrs2@rpi.edu; Farhan Gandhi, gandhf@rpi.edu

ACKNOWLEDGMENTS

This work was sponsored by the Office of Naval Research (ONR), under contract number N00014-16-1-2705.

REFERENCES

[1]Gautam, A., Sujit, P. B., and Saripall, S., "A survey of autonomous landing techniques for UAVs," 2014 International Conference on Unmanned Aircraft Systems (ICUAS), Orlando, FL, May 2014.

[2]Voskuijl, M., Padfield, G. D., Walker, D. J., Manimala, B. J., and Gubbels, A. W., "Simulation of Automatic Helicopter Deck Landings Using Nature Inspired Flight Control," *The Aeronautical Journal*, Vol. 38, (12), August 2010, pp. 25–34.

[3]Ngo, T. D. and Sultan, C., "Model Predictive Control for Helicopter Shipboard Operations in the Ship Airwakes," *Journal of Guidance, Control, and Dynamics*, Vol. 39, (3), 2016, pp. 574–583.

[4]Soneson, G. L., Horn, J. F., Yang, J., and Zheng, A., "Simulation Testing of Advanced Response Types for Ship-Based Rotorcraft," *Journal of the American Helicopter Society*, Vol. 61, (3), July 2016, pp. 1–13.

[5]Horn, J. F., Yang, J., He, C., Lee, D., and Tritschler, J., "Autonomous Ship Approach and Landing Using Dynamic Inversion Control with Deck Motion Prediction," 41st European Rotorcraft Forum, Munich, Germany, September 2015.

[6]Lane, S. and Stengel., R., "Flight control using nonlinear inverse dynamics," *Automatica*, Vol. 24, 1988, pp. 471–483.

[7]Tritschler, J. and Horn, J. F., "Objective Function Development for Optimized Path Guidance for Rotorcraft Shipboard Recovery," AIAA Atmospheric Flight Mechanics Conference, Dallas, TX, June 2015.

[8]Hu, B. and Mishra, S., "A time-optimal trajectory generation algorithm for quadrotor landing onto a moving platform," American Control Conference (ACC), Seattle, WA, June 2017.

[9]Krishnamurthi, J. and Gandhi, F. S., "Flight Simulation and Control of a Helicopter Undergoing Rotor Span Morphing," *Journal of the American Helicopter Society*, Vol. 63, (1), January 2018, pp. 72–91.

[10]Howlett, J. J., "UH-60A Black Hawk Engineering Simulation Program: Volume I - Mathematical Model," NASA CR 166309, 1981.

[11]Schwartz, A., "Systematic Characterization of the Naval Environment (SCONE) Standard Deck Motion Data for a Generic Surface Combatant," Memorandum from office of naval research and naval surface warfare center– carderock division, May 2015.

[12]Cheeseman, I. and Bennett, W., "The Effect of the Ground on a Helicopter Rotor in Forward Flight," ARC R&M 3021, 1955.

[13]Peters, D. and HaQuang, N., "Dynamic Inflow for Practical Applications," *Journal of the American Helicopter Society*, Vol. 33, October 1988, pp. 64–66.

[14]Sparbanie, S., "Modeling and Identification of Unsteady Airwake Disturbances on Rotorcraft," *Ph.D. Thesis, The Pennsylvania State University*, 2008.

[15]Rigatos, G., *Nonlinear Control and Filtering Using Differential Flatness Approaches: Applications to Electromechanical Systems*, Springer, 2015, Chapter 2.